Nuclear Instruments and Methods in Physics Research A 1072 (2025) 170223

Contents lists available at ScienceDirect

Nuclear Inst. and Methods in Physics Research, A

journal homepage: www.elsevier.com/locate/nima

Development of a nonlinear plasma lens for achromatic beam transport

P. Drobniak [a,*], E. Adli [a], H. Bergravf Anderson [a], A. Dyson [b], S.M. Mewes [c], K.N. Sjobak [a], M. Thévenet [c], C.A. Lindstrøm [a]

[a] Department of Physics, University of Oslo, 0316, Oslo, Norway
[b] Department of Physics, University of Oxford, Clarendon Laboratory, Parks Road, OX1 3PU, Oxford, United Kingdom
[c] Deutsches Elektronen-Synchrotron DESY, Notkestr. 85, 22607, Hamburg, Germany

ARTICLE INFO

Keywords:
Active plasma lens
Magnetic focusing
Nonlinear beam optics
Achromatic focusing
Particle accelerator
Plasma-wakefield accelerator
Beam dynamics
Hall effect
Magnetisation
Plasma discharge
Plasma hydrodynamic simulation

ABSTRACT

We introduce the new idea of a nonlinear active plasma lens, as part of a larger transport lattice for achromatic electron beam transport. The proposed implementation uses an external dipole magnet acting on a plasma and is motivated by 1D-hydrodynamic simulations. The manufactured design is presented, including its undergoing experimental characterisation on the CLEAR beam-line at CERN.

1. Introduction

Plasma acceleration [1–4] is a promising technology for next-generation electron accelerators, mainly due to the high gradient they can sustain, orders of magnitude above conventional radio-frequency (RF) cavities. Currently, plasma accelerators typically offer beams with energy ranging from the MeV to a few GeV-level [5], with a few-percent energy spread, from pC to nC of charge, at repetition rate around 10 Hz and duration of a few fs. Such beams may already be promising candidates for applications including radiation therapy with electrons [6] and X-ray free-electron lasers [7]. In order to reach much higher beam-energy gains than the ∼10 GeV available from a single plasma stage, such as the 20–100 GeV required for future strong-field quantum electrodynamics (SFQED) experiments [8] or the TeV-level energies required for particle colliders [9,10], multiple stages must be used [11].

In conventional RF accelerators, a series of quadrupoles is used to keep the beam focused. However, using the same technology to stage plasma accelerators is not suitable due to beam chromaticity. One compact alternative is to use so-called *active plasma lenses* [12,13]. These devices are composed of a volume, filled up with gas, where a longitudinal discharge in the kA-level creates an azimuthal B-field distribution focusing in both planes simultaneously.

A first experimental staging of plasma accelerators was achieved by Steinke et al. in 2016 [14], where two laser-plasma accelerators (one gas-jet injector for the electron source and one discharge capillary for an additional acceleration) were coupled by an active plasma lens. This result represents a key milestone for plasma staging. However, the coupling efficiency was poor, with a few percent of the charge remaining at the end of the line. One origin for this is the *chromatic* behaviour of the lens [15], focusing each beam energy at different focal lengths.

To solve this issue, an *achromatic* lattice has been proposed [16], as described in Fig. 1. It requires two nonlinear plasma lenses, described in more detail below. The detailed working principle of the lattice is the main topic of an upcoming publication.

This article describes the planning and preliminary results of the development, both theoretical and experimental, of a nonlinear plasma lens – a key part of the ERC project SPARTA [17]. Section 2 introduces the general idea of a nonlinear plasma lens, useful for the achromatic lattice proposed in Fig. 1 together with potential solutions to realise it. Hydrodynamic simulations are then presented (Section 3), which motivate the idea proposed in Section 2. The design we developed is described (Section 4) and the external B-field distribution required by the design is simulated and measured (Section 5). Lastly, the lens

* Corresponding author.
E-mail address: pierre.drobniak@fys.uio.no (P. Drobniak).

https://doi.org/10.1016/j.nima.2025.170223
Received 1 November 2024; Received in revised form 9 January 2025; Accepted 10 January 2025
Available online 17 January 2025

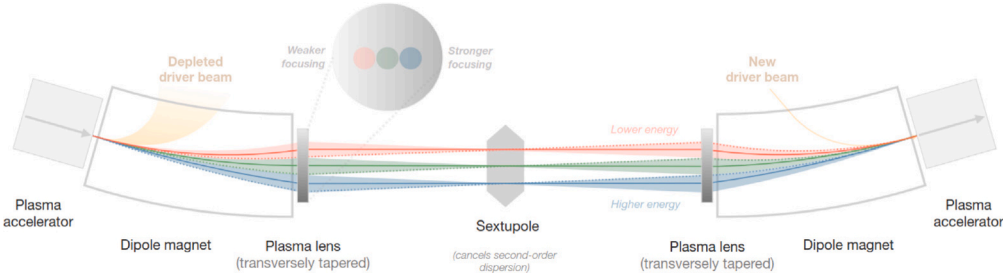

Fig. 1. Schematic layout of an achromatic lattice using dipole magnets to disperse the beam onto a nonlinear plasma lens, which focusing strength varies transversely, and is tuned such that the focal length is equal for all energies (same distance to the focus point, i.e. achromatic focusing). A mirror symmetric setup ensures that both nonlinear forces as well as the dispersion is canceled. The central sextupole is used to cancel the second-order energy dependence of the offset and angle of the bunch at the end of the lattice (i.e., cancelling the second-order dispersion).
Source: From Ref. [16].

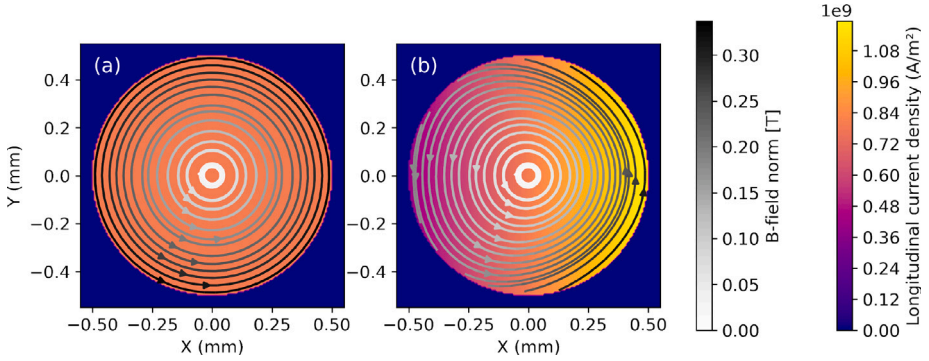

Fig. 2. Theoretical B-field distribution in the linear case (a) and nonlinear non-radially-symmetric case (b). A circle with radius 500 µm is added to indicate the capillary walls. Coefficients for the plots are: $g_0 = 500\,\mathrm{T/m}$, $D_x = 1\,\mathrm{mm}$ (note that this is exaggerated by a factor 10 or so for better visibility of the nonlinearity).

characterisation is presented (Section 6), as well as an outlook towards the next steps of the project (Section 7).

2. The nonlinear plasma lens

An "ideal" plasma lens, known as a *linear* plasma lens, has a longitudinal current density that is transversely uniform $\vec{j_0} = j_{0,z}\vec{e_z}$ within the circular aperture of the lens. Using Ampère-Maxwell's law $\nabla\vec{B} = \mu_0\vec{j}$ (with $\vec{j}$ being the current density), we get a purely azimuthal field [see Fig. 2(a)], linearly growing with the distance from axis:

$$B_x^{\mathrm{lin}} = -\,g_0 y \tag{1}$$

$$B_y^{\mathrm{lin}} = +\,g_0 x \tag{2}$$

with $g_0 = \mu_0\|\vec{j_0}\|/2$ the focusing gradient for this case.

However, the current density is not always uniform. Cooling at the lens walls leads to a hotter core with a higher conductivity ($j \propto E\sigma \propto T^{3/2}$ [18,19], with E the electric field, σ the electrical conductivity and T the temperature), so a nonuniform distribution of the current density (validated experimentally [20,21]). This causes the lens to be nonlinear (nonlinear focusing strength), but still with an azimuthal symmetry.

While the above indicates the possibility of nonlinear plasma lenses, it is not a suitable nonlinearity for the achromatic lattice in Fig. 1. We suppress this temperature-induced radial nonlinearity by working with a heavier gas, such as argon, and thus break the assumption of radial thermal steady-state, as proposed by Lindstrøm et al. [21]. The motivation of this article is to propose a nonlinear lens with focusing strength varying in *one* direction (x) and constant in the other direction (y) (see Fig. 1). Let us consider a beam, dispersed in x by a dipole (Fig. 1) with dispersion D_x. The centroid of each energy slice of the beam thus enters the lens with a different x-position. In order to provide the same focal length to each energy component, the focusing gradient must be $g(x,y) = g_0(1 + x/D_x)$. The distribution satisfying such a condition is:

$$B_x^{\mathrm{nonlin}} = -g_0\left(y + \frac{1}{D_x}xy\right) \tag{3}$$

$$B_y^{\mathrm{nonlin}} = +g_0\left(x + \frac{1}{D_x}\frac{x^2+y^2}{2}\right). \tag{4}$$

Typical values for g_0 are in the 100–1000 T/m range and we want $1/D_x$ values around 1%–10% per lens radius (i.e., around $\sim$ 100 m for a typical 1 mm-diameter lens). The shape of the corresponding field is displayed in Fig. 2, where the current is added in the background. The plasma lens described here (non-azimuthally symmetric) will from now on be referred to as *nonlinear*.

Our proposed solution to obtain this B-field distribution is to make use of the Hall effect, inspired by Kunkel [22]. An external B-field $\vec{B}_{ext}$ is applied to a plasma which reacts by re-arranging its electron density n_e transversely (Hall effect), as presented in Fig. 3.

Since the current density $\vec{j}$ depends on the temperature T_e, which again depends on the electron density n_e, if one acts on n_e, one may produce a nonuniform current density. In addition to the Hall-effect, we have to bear in mind that adding up a vertical dipole field increases the total B-field (plasma + external field) on one side of the capillary and decreases it on the other, thus breaking the axial symmetry of B. Since the magnitude of the transverse B-field impacts the plasma electrical conductivity (magnetisation of the plasma [23]), this will impact the redistribution of j_z. Optimally, a current density which is linearly dependent on x is required to satisfy Eqs. (3) and (4):

$$j_z^{\mathrm{nonuni}} = \frac{2g_0}{\mu_0}(1 + \frac{1}{D_x}x). \tag{5}$$

3. Simulation

Hydrodynamic simulations were performed in collaboration with DESY, using a modified version of the COMSOL simulation framework

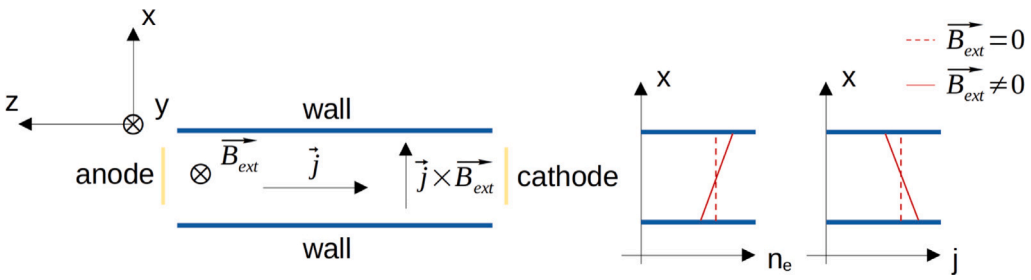

Fig. 3. Principles of the Hall effect in a plasma. The external B-field $\vec{B}_{ext}$ acts on the current $\vec{j}$ through the Lorentz force $\vec{j}\times\vec{B}_{ext}$. The theoretical effect on the electron density n_e and j is added, assuming that $j \propto 1/n_e$. Based on Kunkel (1981) [22].

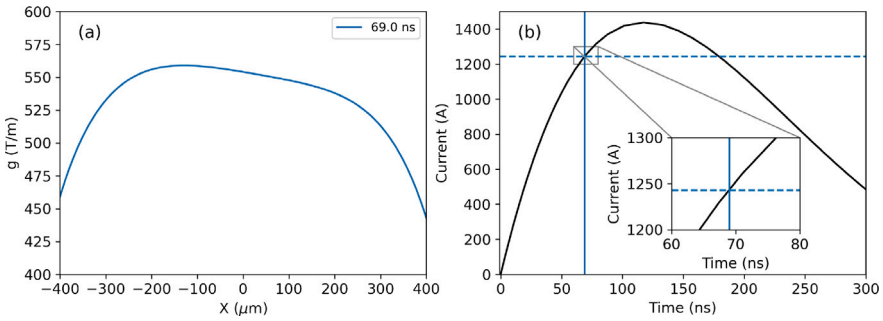

Fig. 4. COMSOL hydrodynamics simulation results in 1D displaying: (a) the focusing strength $g = dB_y/dx$ and (b) the current profile used as input in the simulation. The species used is H_2, at 13 mbar, and is fully ionised at the time-step presented in (a). The capillary is 1 mm wide. The external B-field is along y and set to 10 mT.

presented in [24]. It models the ionisation of a gas (currently only H_2) from a time-varying input current. The plasma is modelled as a single fluid, in a non-equilibrium reaction system (ionisation and recombination modelled), with two temperatures, one for the electrons and one for the "heavies" (ions and neutrals). Working with a 1D-Cartesian model assumes slab geometry, i.e., that the capillary is infinitely long and infinitely wide (in y for instance). We assume longitudinal uniformity, which is a reasonable approximation given the aspect ratio of the cell (much longer than wide) and the short timescale (no time for plasma expulsion) [25,26]. As of yet, only preliminary 1D-simulations (in x) have been performed (for computation cost reasons), where we added the external B-field (in y) in search for a non-radially-symmetric nonlinearity in B.

First simulation results are presented in Fig. 4. Within a transverse window of $[-150, +150]$ μm, the value of g lies around 550 T/m, with an x-derivative corresponding to a linear term matching a D_x of 10 mm, which is what we wish to achieve. The observed nonlinear B-distribution (linear g) originates from both the Hall effect and plasma magnetisation.

Outside of the $[-150, +150]$ μm window, the distribution of g starts dropping, which originates from the fast thermal dynamics of H_2 (already observed experimentally without external B-field [21]), transversely rearranging close to a thermal steady-state. We think this could be mitigated by using a heavier gas. A model for this is currently under development, which is more complex than for hydrogen since a heavier gas has more ionisation states. In addition, we aim to implement 2D x-y simulations within 2025 to better capture the effects of the transverse geometry.

4. Hardware design

A new plasma-lens design is presented in Fig. 5. This was developed and manufactured at the University of Oslo, in collaboration with the Instrumentation Laboratory (I-Lab).

It is composed of a capillary, held between two electrodes (a tubular capillary setup inspired by recent designs from DESY [27]). Gas is injected on both sides, and a vertically aligned external B-field is generated by an electromagnet surrounding the capillary. A small mirror (OTR screen) is attached close to the entrance electrode for alignment and beam-size measurements. In order to avoid sparking between the conducting surfaces of the electrodes and the magnet poles (only a few mm apart), we covered the magnet poles with 3D-printed insulating material. The entire assembly is supported by a PEEK holder, for integration to the flange of a vacuum chamber. For compactness and easy mounting, the gas pipes (approx. 1 m each) that feed the capillary are supported by 3D-printed pipe holders.

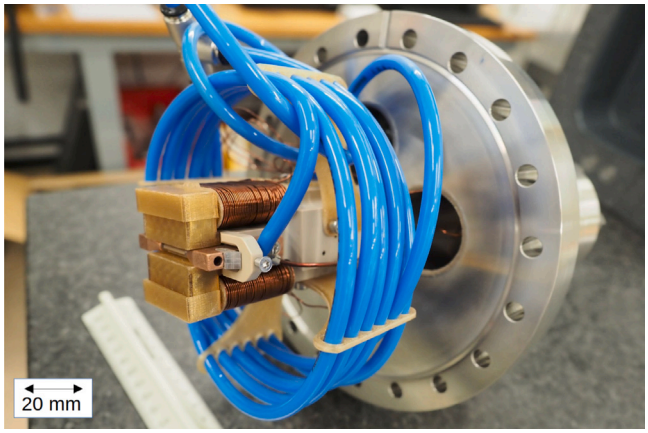

Fig. 5. Plasma-lens design developed at the University of Oslo and prepared for integration in the CLEAR beam-line. The capillary is held between two electrodes (copper) and an external electromagnet creates the external B-field for generating the Hall effect in the plasma. Gas is injected on each side of the capillary through channels inside of hollow electrodes. The 45°-tilted mini-OTR screen used for alignment is visible in grey, next to the hollow entrance electrode, with its fiducials used for alignment.

5. External B-field distribution

In order to assess the validity of our electromagnet design, we performed magnetostatic simulations with COMSOL [28], with the aim

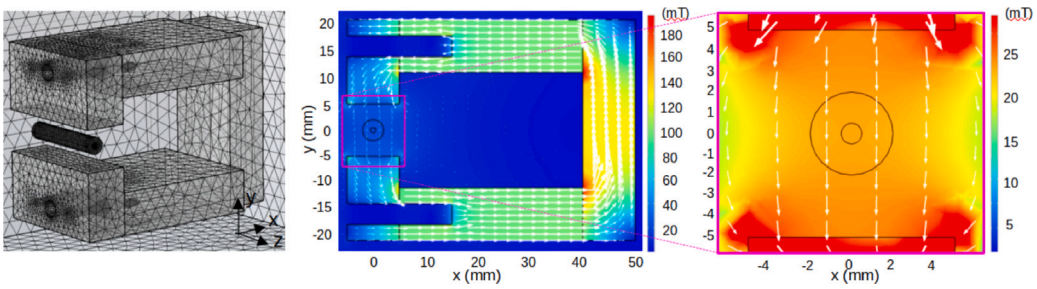

Fig. 6. COMSOL [28] magnetostatic simulation results of the electromagnet design.

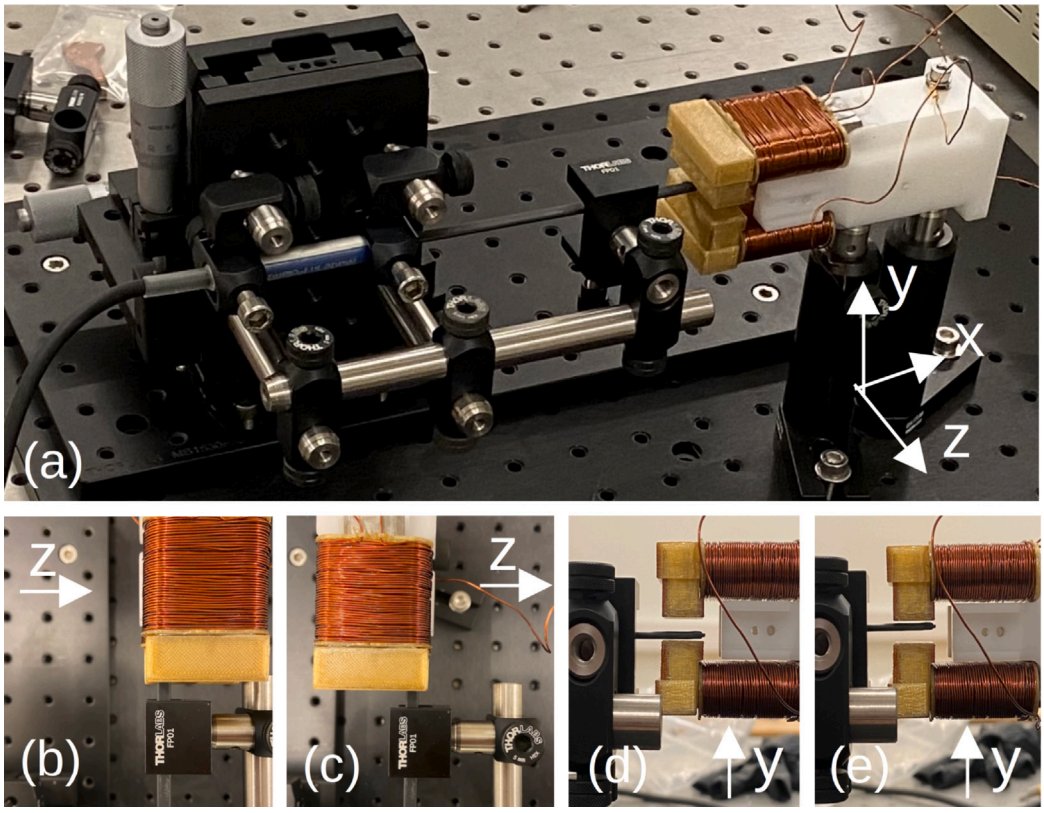

Fig. 7. Set-up used at the University of Oslo for external B-field characterisation: (a) set-up with magnetic probe, translation stage and electromagnet, (b–c) two extreme scan positions in z, (d–e) two extreme scan positions in y (xz-planes).

to ensure a uniform and vertical (along y) external B-field distribution. The model is built by assuming a uniform magnetisation of each arm (upper and lower) of the yoke.

Simulation results for a B-field of 100 mT inside the yoke (theoretically achievable with a small current in the coils and low permeability material) in each arm are presented in Fig. 6.

At the location of the capillary, the external B-field remains vertical and its value is constant 23.2 ± 0.2 mT. Compared to the 10 mT from our hydrodynamic simulations, this value is satisfactory. The transfer from yoke arm to capillary is from 100 mT to 23.2 mT, so roughly 23%.

The simulation-generated values given above have been cross-checked using a set-up at the University of Oslo, presented in Fig. 7. The B-field is measured using a Hall-probe (ASONIK type SMS-102, radial), with precision of 0.1 mT. It is mounted on a 3-axis translation stage, with 1 μm precision. Each solenoid consists of 2 winding layers, ensuring a total winding density in each solenoid of $n_{\mathrm{sol}} = 2400$ turns/m. The solenoids are connected in series and the current is set on the DC-power source to $I_{\mathrm{sol}} = 1.5 \pm 0.01$ A. The field generated by each solenoid in vacuum is calculated from the formula $B_{\mathrm{sol,vac}} = \mu_0 n_{\mathrm{sol}} I_{\mathrm{sol}} = 4.45$ mT. Measurements are performed between the poles, without capillary and without electrodes (should not deviate from the final set-up, since copper is not magnetic). The measurement space steps in $[x, y, z]$ are [0.1, 1,5] mm. Since the absolute position of the B-field sensor was not known exactly, we calibrated our experiment by identifying the opposite positions where the B-field started to drop equally, and took the centre of these points as the set-up centre.

Measurements results are presented in Fig. 8. The vertical B-field has a mean value of 26.4 mT, with variations up to 2% within the capillary area defined in the figure.

Regarding the uniformity, the experimental measurement shows a satisfactory level of field uniformity in the plasma region, validating the magnetostatic COMSOL simulation to a few percent. Further simulations of plasma hydrodynamics and beam transport are however necessary to validate the effect of the provided level of external B-field uniformity.

6. Experimental setup in the CLEAR user facility at CERN

In order to directly measure the B-field distribution generated by our nonlinear plasma lens, we plan to use an external relativistic electron beam and measure its deflection by the lens. As already proposed

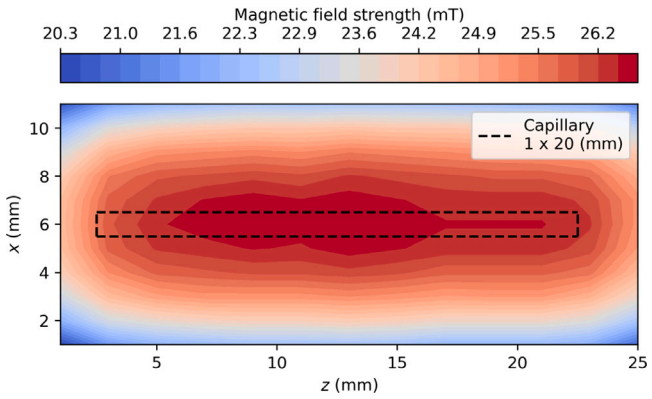

Fig. 8. Vertical B-field measurement at the plane in y corresponding to the capillary centre, performed without electrodes and without capillary. The virtual position of the capillary is added in dashed black.

and performed in [29], such a way to proceed allows to compute back the lens field. The angular deflection at the cell exit is measured as a transverse displacement on a downstream screen $(\Delta x, \Delta y)$, as a function of the lens offset (x_l, y_l) with regards to the beam axis [with the point $(0,0)$ corresponding to the centre of the lens coinciding with the beam axis]. Within the thin lens approximation, it can be expressed as follows [21]:

$$\Delta x(x_l, y_l) = +\frac{ecL\Delta s}{E} B_y(x_l, y_l) \tag{6}$$

$$\Delta y(x_l, y_l) = -\frac{ecL\Delta s}{E} B_x(x_l, y_l) \tag{7}$$

with e the electron charge, c the speed of light in vacuum, L the cell length, Δs the distance from the capillary centre to the screen and E the beam energy (assuming ultra-relativistic beam particles).

The first step presented in this Section 6.1 ensures that the design can be integrated in a beam-line, i.e., is vacuum-compatible and does not spark outside of the capillary. Section 6.2 describes the measurement of B (sum of external field B_{ext} and pure discharge field B_{dis}).

6.1. Commissioning of the plasma lens

We are performing the measurement at CLEAR at CERN [30,31], offering electron with the following characteristics: 60–200 MeV energy, 0.01–50 nC charge, 1–100 bunches per pulse, 1–10 pulses per second, 1 ps–50 ns pulse length, and a focus down to 50×50 µm at the plasma-lens entrance. The lens integrated in the beam-line is shown in Fig. 9.

The commissioning has proven the validity of the design in terms of gas injection and sparking. Tested with argon, the pressure in the upstream gas buffer is set to approx. 20 mbar. Assuming 70% pressure loss, as measured previously [21], this implies ∼6 mbar in the capillary. The pressure in the vacuum chamber remains low enough for the secondary turbopump to remain at full speed. No discharge outside of the capillary was observed during operation. The discharge, around 1 kA, shows a time-jitter below 5 ns.

6.2. Planning the plasma-lens characterisation

The second step of the experiment is the lens characterisation, i.e., measurement of the total field B (sum of B_{ext} from the electromagnet and B_{dis} from the discharge).

Among the possible scans in the xy-plane, the most qualitatively visible outcome appears for a vertical scan centred on the lens axis. Here we approximate the geometrical axis to be also the magnetic axis, i.e., we neglect the constant axis-shift induced by the electromagnet through B_{ext}. The scan positions are $(0, y_l)$, with resulting positions on the screen downstream described as follows (from Eqs. (8) and (9)):

$$\Delta x(0, y_l) = \frac{ecL\Delta s}{2E} g_0 \frac{y_l^2}{D_x} \tag{8}$$

$$\Delta y(0, y_l) = \frac{ecL\Delta s}{E} g_0 y_l. \tag{9}$$

Rough estimates using numbers from CLEAR, operating at maximum vertical offset, gives horizontal offsets on the screen of approximately 50–100 µm (while the vertical offset on the screen is 2–3 mm). Tracking simulations were performed and the simulated results of such a scan are presented in Fig. 10. A clear "banana"-shape appears, which will be a key indicator of the nonlinearity.

The full characterisation of the lens requires a "grid"-scan of the entire xy-plane. As a beginning, however, we focus on the demonstration of the nonlinearity.

7. Conclusion and outlook

In this article, we are proposing an active nonlinear plasma lens design, as part of a lattice for achromatic beam transport. The solution proposed to generate the nonlinearity is to use an external B-field and is supported by 1D hydrodynamics simulations in H_2 showing the impact of magnetisation and Hall effect on the resulting total B-field

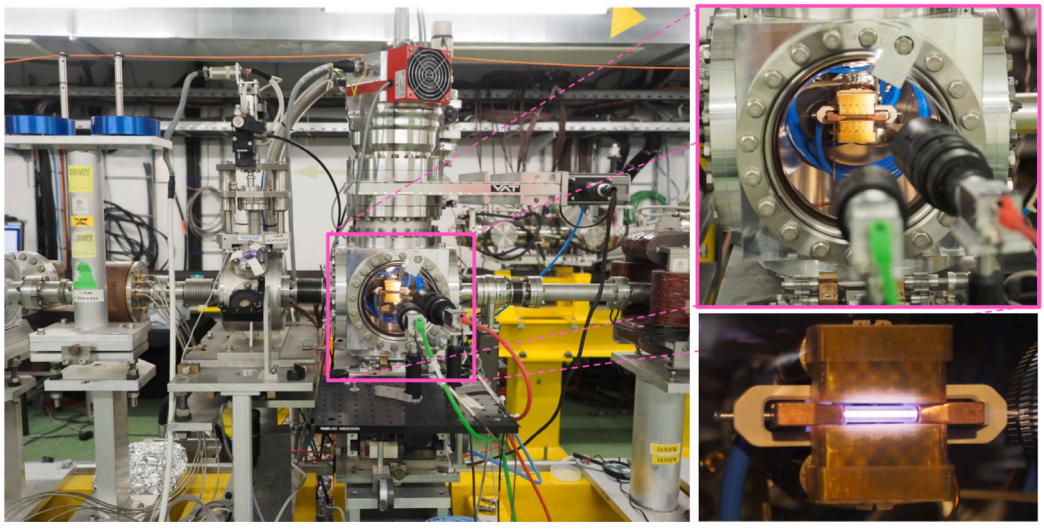

Fig. 9. Pictures of the nonlinear plasma lens integrated in the CERN CLEAR beam-line in September 2024. The electron beam goes from right to left.

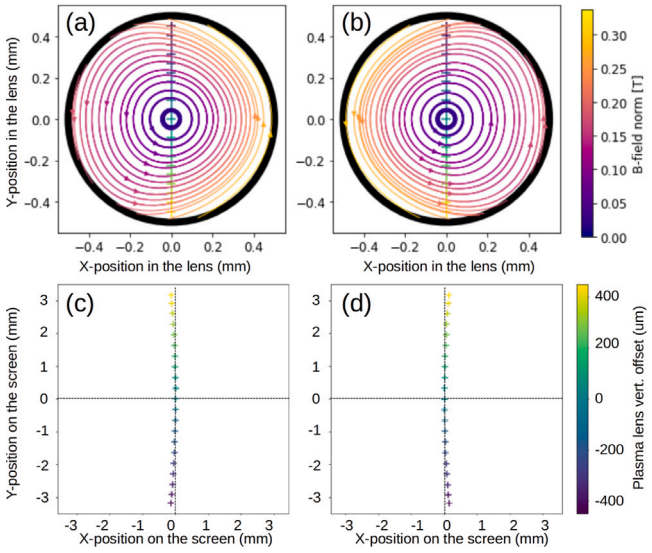

Fig. 10. Simulated results emulating an experiment with a 1 mm diameter capillary with: (a–b) theoretical B-field distribution in the lens with accentuated $1/D_x$ set to 10 %/mm instead of 1 %/mm for better visualisation of the nonlinearity, (c–d) predicted observation from tracking simulations on the screen downstream of the lens for an actual nonlinear factor $1/D_x = 10\,\%/\mathrm{mm}$. The points scanned are displayed as crosses in all sub-graphs. The effect of the external field B_{ext} from the electromagnet is neglected, resulting in a magnetic centre coinciding with the cell geometrical centre.

distribution. The design developed at the University of Oslo is presented and the external B-field generated by the electromagnet is simulated and experimentally measured. The characterisation of the full B-field distribution (i.e., the sum of the external field from the electromagnet and the magnetic field from the discharge current) inside the lens is planned to be conducted at CLEAR.

A preliminary experiment was already carried out in Sep. 2024 and results are under analysis. The objective at this stage is to experimentally observe and quantify a nonlinearity in focusing strength. In the medium-term, the lens should be used to focus a dispersed beam and prove its ability to match each energy component of the beam. Longer term, our lens design could experimentally validate the concept of achromatic transport when tested with the full lattice.

Declaration of competing interest

The authors declare that they have no known competing financial interests or personal relationships that could have appeared to influence the work reported in this paper.

Acknowledgements

The SPARTA project is funded by the European Union (ERC, SPARTA, 101116161). We acknowledge Sigma2 - the National Infrastructure for High-Performance Computing and Data Storage in Norway for awarding this project access to the LUMI supercomputer, owned by the EuroHPC Joint Undertaking, hosted by CSC (Finland) and the LUMI consortium. The work was also supported by the Research Council of Norway (NFR Grants No. 313770 and 310713).

We greatly thank: the workshop I-Lab at the University of Oslo (J. S. Ringnes, S. R. Solbak, H. Borg) for their help in designing and manufacturing of the assembly and CERN for facilitating beam time at CLEAR (R. Corsini, W. Farabolini, A. Gilardi, P. Korysko, V. Rieker).

References

[1] V.I. Veksler, Coherent Principle of Acceleration of Charged Particles, CERN, 1956, p. 80.
[2] T. Tajima, J.M. Dawson, Laser electron accelerator, Phys. Rev. Lett. 43 (1979) 267–270.
[3] P. Chen, J.M. Dawson, R.W. Huff, T. Katsouleas, Acceleration of electrons by the interaction of a bunched electron beam with a plasma, Phys. Rev. Lett. 54 (1985) 693–696.
[4] R.D. Ruth, A.W. Chao, P.L. Morton, P.B. Wilson, A plasma wake field accelerator, Part. Accel. 17 (1985) 171–189.
[5] A. Gonsalves, K. Nakamura, J. Daniels, C. Benedetti, C. Pieronek, T. De Raadt, S. Steinke, J. Bin, S. Bulanov, J. van Tilborg, et al., Petawatt laser guiding and electron beam acceleration to 8 GeV in a laser-heated capillary discharge waveguide, Phys. Rev. Lett. 122 (2019) 084801.
[6] L. Labate, et al., Toward an effective use of laser-driven very high energy electrons for radiotherapy: Feasibility assessment of multi-field and intensity modulation irradiation schemes, Sci. Rep. 10 (2020) 17307.
[7] D.O. Espinos, High Quality Laser Driven Electron Beams for Undulator and Free Electron Laser Radiation (Ph.D. thesis), Université Paris-Saclay; Ōsaka University. Faculty of Engineering, 2021.
[8] H. Abramowicz, et al., Conceptual design report for the LUXE experiment, Eur. Phys. J. Spec. Top. 230 (2021) 2445–2560.
[9] V. Shiltsev, F. Zimmermann, Modern and future colliders, Rev. Modern Phys. 93 (2021) 015006.
[10] B. Foster, R. D'Arcy, C.A. Lindstrøm, A hybrid, asymmetric, linear Higgs factory based on plasma-wakefield and radio-frequency acceleration, New J. Phys. 25 (2023) 093037.
[11] C.A. Lindstrøm, Staging of plasma-wakefield accelerators, Phys. Rev. Accel. Beams 24 (2021).
[12] W.K.H. Panofsky, W.R. Baker, A focusing device for the external 350-Mev proton beam of the 184-inch cyclotron at berkeley, Rev. Sci. Instrum. 21 (1950) 445–447.
[13] J. van Tilborg, et al., Active plasma lensing for relativistic laser-plasma-accelerated electron beams, Phys. Rev. Lett. 115 (2015) 184802.
[14] S. Steinke, J. van Tilborg, C. Benedetti, C. Geddes, C. Schroeder, J. Daniels, K. Swanson, A. Gonsalves, K. Nakamura, N. Matlis, et al., Multistage coupling of independent laser-plasma accelerators, Nature 530 (2016) 190–193.
[15] M. Migliorati, A. Bacci, C. Benedetti, E. Chiadroni, M. Ferrario, A. Mostacci, L. Palumbo, A.R. Rossi, L. Serafini, P. Antici, Intrinsic normalized emittance growth in laser-driven electron accelerators, Phys. Rev. ST Accel. Beams 16 (2013).
[16] C.A. Lindstrøm, et al., manuscript in preparation.
[17] European Commission, Staging of plasma accelerators for realizing timely applications, 2023, http://dx.doi.org/10.3030/101116161.
[18] N.A. Bobrova, A.A. Esaulov, J.-I. Sakai, P.V. Sasorov, D.J. Spence, A. Butler, S.M. Hooker, S.V. Bulanov, Simulations of a hydrogen-filled capillary discharge waveguide, Phys. Rev. E 65 (2001).
[19] J. van Tilborg, et al., Nonuniform discharge currents in active plasma lenses, Phys. Rev. Accel. Beams 20 (2017) 032803.
[20] J.-H. Röckemann, et al., Direct measurement of focusing fields in active plasma lenses, Phys. Rev. Accel. Beams 21 (2018).
[21] C.A. Lindstrøm, et al., Emittance preservation in an aberration-free active plasma lens, Phys. Rev. Lett. 121 (2018) 194801.
[22] W. Kunkel, Hall effect in a plasma, Am. J. Phys. 49 (1981) 733–738.
[23] J. Davies, H. Wen, J.-Y. Ji, E.D. Held, Transport coefficients for magnetic-field evolution in inviscid magnetohydrodynamics, Phys. Plasmas 28 (1) (2021).
[24] S.M. Mewes, G. Boyle, A.F. Pousa, R. Shalloo, J. Osterhoff, C. Arran, L. Corner, R. Walczak, S. Hooker, M. Thévenet, Demonstration of tunability of HOFI waveguides via start-to-end simulations, Phys. Rev. Res. 5 (2023) 033112.
[25] G. Bagdasarov, P. Sasorov, V. Gasilov, A. Boldarev, O. Olkhovskaya, C. Benedetti, S. Bulanov, A. Gonsalves, H.-S. Mao, C.B. Schroeder, et al., Laser beam coupling with capillary discharge plasma for laser wakefield acceleration applications, Phys. Plasmas 24 (8) (2017).
[26] G. Bagdasarov, K. Kruchinin, A.Y. Molodozhentsev, P. Sasorov, S. Bulanov, V. Gasilov, Discharge plasma formation in square capillary with gas supply channels, Phys. Rev. Res. 4 (1) (2022) 013063.
[27] J. Wood, et al., Progress towards high-quality, high-repetition-rate plasma acceleration at FLASHForward, in: Proc. IPAC'24.
[28] COMSOL, Inc., COMSOL Multiphysics® v. 5.6, 2021, Software.
[29] K.N. Sjobak, E. Adli, R. Corsini, W. Farabolini, G. Boyle, C.A. Lindstrø m, M. Meisel, J. Osterhoff, J.-H. Röckemann, L. Schaper, et al., Strong focusing gradient in a linear active plasma lens, Phys. Rev. Accel. Beams 24 (2021) 121306.
[30] D. Gamba, R. Corsini, S. Curt, S. Doebert, W. Farabolini, G. Mcmonagle, P. Skowronski, F. Tecker, S. Zeeshan, E. Adli, C. Lindstrøm, A. Ross, L. Wroe, The CLEAR user facility at CERN, Nucl. Instrum. Methods Phys. Res. Sec. A 909 (2018) 480–483.
[31] K.N. Sjobak, et al., Status of the CLEAR electron beam user facility at CERN, in: Proc. IPAC'19, 2019, pp. 983–986.